HHS Public Access

Author manuscript

J Struct Biol. Author manuscript; available in PMC 2016 February 01.

Published in final edited form as:

J Struct Biol. 2015 February ; 189(2): 123–134. doi:10.1016/j.jsb.2014.11.008.

Sparse and incomplete factorial matrices to screen membrane protein 2D crystallization

R. Lasala[1,#], **N. Coudray**[1,#], **A. Abdine**[2,#], **Z. Zhang**[1], **M. Lopez-Redondo**[3], **R. Kirshenbaum**[2], **J. Alexopoulos**[3], **Z. Zolnai**[4], **D.L. Stokes**[1,3], and **I. Ubarretxena-Belandia**[1,2,*]

[1]New York Structural Biology Center, 89 Convent Avenue, New York, NY 10027, USA

[2]Department of Structural and Chemical Biology, Icahn School of Medicine at Mount Sinai, 1425 Madison Avenue, New York, NY 10029, USA

[3]Skirball Institute of Biomolecular Medicine and Department of Cell Biology, New York, University School of Medicine, 540 First Avenue, New York, NY 10016, USA

[4]Department of Biochemistry, University of Wisconsin-Madison, 433 Babcock Drive, Madison, WI 53706, USA

Abstract

Electron crystallography is well suited for studying the structure of membrane proteins in their native lipid bilayer environment. This technique relies on electron cryomicroscopy of two-dimensional (2D) crystals, grown generally by reconstitution of purified membrane proteins into proteoliposomes under conditions favoring the formation of well-ordered lattices. Growing these crystals presents one of the major hurdles in the application of this technique. To identify conditions favoring crystallization a wide range of factors that can lead to a vast matrix of possible reagent combinations must be screened. However, in 2D crystallization these factors have traditionally been surveyed in a relatively limited fashion. To address this problem we carried out a detailed analysis of published 2D crystallization conditions for 12 β-barrel and 138 α-helical membrane proteins. From this analysis we identified the most successful conditions and applied them in the design of new sparse and incomplete factorial matrices to screen membrane protein 2D crystallization. Using these matrices we have run 19 crystallization screens for 16 different membrane proteins totaling over 1,300 individual crystallization conditions. Six membrane proteins have yielded diffracting 2D crystals suitable for structure determination, indicating that these new matrices show promise to accelerate the success rate of membrane protein 2D crystallization.

*Address correspondence to: Iban Ubarretxena-Belandia, Dept. Structural and Chemical Biology, Icahn School of Medicine at Mount Sinai, Icahn Medical Institute Bldg., Room 16-70E, 1425 Madison Avenue, Box 1677, New York, NY 10029, Office: +1-212-659-5593, Fax: +1-212-849-2456, Iban.Ubarretxena@mssm.edu.

#Equal contributions

Keywords

Two-dimensional (2D) crystal; membrane protein; electron crystallography; high-throughput screening; membrane protein reconstitution; electron cryomicroscopy; 96-well format

1. Introduction

Membrane protein electron crystallography was pioneered in the 1970s by Henderson and Unwin through their studies of bacteriorhodopsin (Henderson and Unwin, 1975), and relies on electron cryomicroscopy (cryo-EM) of two-dimensional (2D) crystalline specimens of membrane proteins in a lipid bilayer. This method is thus ideal for studying the structure of membrane proteins in their natural membrane environment (Ubarretxena-Belandia and Stokes, 2010;Ubarretxena-Belandia and Stokes, 2012). As in X-ray crystallography, growing suitable crystals represents one of the major bottlenecks in the application of this technique. 2D crystals are typically grown by reconstitution of purified, detergent-solubilized membrane proteins into lipid bilayers at a high enough density to favor the formation of a regular array (Jap et al., 1992;Kühlbrandt, 1992;Mosser, 2001). Several methods, including dialysis (Kühlbrandt, 1992), controlled dilution (Remigy et al., 2003), adsorption onto a hydrophobic resin (Rigaud et al., 1997) or complexation with cyclodextrins (Signorell et al., 2007) are generally employed for detergent removal and reconstitution of the protein into proteoliposomes. Identifying the conditions for growing 2D crystals requires screening over a wide range of factors including pH, temperature, lipid composition, lipid-to-protein ratio, detergent, amphiphiles, mono- and divalent-ions, inhibitors and ligands. A systematic screen over all of these factors generates a huge matrix of possible reagent combinations, which should ideally be sampled to cover the majority of 2D crystallization space. For 3D crystallization, a vast portion of crystallization space can be screened efficiently and rapidly using sparse (Jancarik et al., 1991;Rupp and Wang, 2004) and incomplete factorial crystallization matrices (Carter Jr, 1990;Gorrec et al., 2011) in combination with high-throughput approaches. In contrast, factors relevant for 2D crystallization have traditionally been surveyed in a relatively limited fashion, potentially missing truly optimal conditions, or in some cases failing to even obtain crystals. However, the recent development of high-throughput tools for 2D crystallization (Cheng et al., 2007;Vink et al., 2007;Coudray et al., 2008;Hu et al., 2010;Iacovache et al., 2010;Karathanou et al., 2010;Kim et al., 2010;Coudray et al., 2011) make it now possible to conduct 2D crystallization trials at a higher pace and reproducibility, and moreover, sufficient amount of data is now available on membrane protein 2D crystallization (reviewed in (Abeyrathne et al., 2012)) to allow the rational design of new and more comprehensive 2D crystallization screens. To this end we first built a 2D crystallization database with information mined from successful 2D crystallization conditions reported in the literature. We analyzed this information to evaluate the effect of the different crystallization factors, and from this analysis we designed new sparse and incomplete factorial matrices to screen membrane protein 2D crystallization. Using these matrices we have been able to grow 2D crystals suitable for structure determination for several membrane proteins.

2. Materials and methods

2.1 2D crystallization database

To construct a database of 2D crystallization experiments we mined the successful conditions from ~250 2D crystallization screens published in ~200 journal articles. To guide us in our literature search we used a recent review by Abeyrathne et al. (Abeyrathne et al., 2012), which tabulated all the membrane proteins studied by electron crystallography up to the year 2012. We tabulated all crystallization conditions according to different factors including pH, temperature, lipid composition, lipid-to-protein ratio, detergent, amphiphiles, and mono- and divalent-ions, along with their respective concentrations. We completed this database with additional fields to describe particular properties of the membrane protein, detergent, and lipid that constitute the initial ternary mixture in a typical 2D crystallization experiment. The 2D crystallization conditions were analyzed by constructing a series of bar charts showing the number of entries in the database as a function of individual crystallization factors.

2.2 Design of a sparse matrix 2D crystallization screen

To design the screen in an unbiased manner we applied the k-means algorithm to form 10 groups using 94 successful 2D crystallization conditions from 57 unique membrane proteins. These conditions were chosen to be as non-redundant as possible. The input fields for the algorithm were: phospholipids characterized by their alkyl chain length and headgroup composition (in percentages of Phosphatidylcholine (PC), Phosphatidylethanolamine (PE), Phosphatidylglycerol (PG), Phosphatidic acid (PA), Phosphatidylserine (PS), Cardiolipin (CA) and E.coli polar lipid extract), pH, NaCl and $MgCl_2$ concentration, and temperature characterized by its median value and variation (which is non-zero when temperature cycling is used).

2.3 Design of an incomplete factorial 2D crystallization screen

The design of so called “incomplete factorial screens” or “grid screens” relies on three major rules: 1) the level of the different factors are assigned randomly; 2) first-order interactions of the level should be balanced; 3) redundancy should be avoided so setups are as different as possible (Carter and Carter, 1979). In order to design a comprehensive incomplete factorial 2D crystallization screen we first identified the ten main factors affecting 2D crystallization, each one of which represents an axis in a ten-dimensional crystallization space. Second, we assigned discrete levels for each factor that then represent points along the corresponding axis. We note that the low occurrence of some of these levels in the database may not reflect the fact that they are not successful, but rather that they have been rarely used. Nevertheless, these levels have been included in the design of the incomplete factorial matrix. For instance, lipid composition is represented by one axis and the levels include commonly used lipids, such as DMPC, DOPC and E.coli lipid extracts, as well as seldom used lipids like DOPG. This approach ensures coverage of a wide range of lipid headgroups, chain lengths and degree of unsaturation. To be compatible with the conventional high-throughput format of 96 conditions per run, our incomplete factorial matrix consisted of 90 conditions (corresponding to points in the ten-dimensional space) plus 6 spots for controls. The 90 points were randomly selected with two constraints: each level should be represented the

same number of times and second-order interactions were balanced to avoid redundancy. For instance, the second constraint forced a given lipid to be combined with a multitude of pHs. In this manner over 20,000 trial matrices were generated. In order to identify one matrix covering the largest amount of ten-dimensional space we computed the standard deviation (SD) of the nearest neighbor-distance (nnd). More specifically, for each of the 90 conditions we computed nnd values relative to the remaining 89 conditions. We note that, because we minimized redundancy during generation of the trial matrices, none of the conditions were identical and thus the nnd values were always > 0. As a consequence, if the conditions were equidistant from each other in ten-dimensional space, then the nnd values would be equivalent and the SD(nnd) would be zero. Following this argument, the matrix with the lowest SD(nnd) represents the most dispersed matrix, i.e., the matrix that most effectively samples the ten-dimensional crystallization space.

2.4 Lipids, detergents and Proteins for 2D crystallization screens

Lipids supplied as powder were purchased from Avanti Polar Lipids (Alabaster, AL) and detergents were bought from Anatrace (Maumee, OH). Detergent solubilized lipid stocks, at a final lipid concentration of 2mg/ml, were prepared in distilled water by first resuspending the lipid at 10mg/ml, and then mixing a 200μl aliquot from this suspension with 800μl of aqueous solution containing detergent. As previously described (Kim et al., 2010), turbidity measurements were employed to determine the minimal detergent concentration needed to solubilize each lipid species. These detergent solubilized lipid stocks could be stored at 4°C for up to four days, or frozen at −80°C for long-term storage.

Sixteen different membrane proteins were expressed and purified either in our own laboratories or in collaborating laboratories. These proteins were usually expressed with either N- or C-terminal affinity-tags to allow purification by affinity chromatography. Generally, the linker region between the tag and the target protein included a TEV or thrombin proteolytic site and, when possible, the tag was removed by proteolysis. The stability, polydispersity, and oligomeric state in detergent for some of these membrane proteins was determined using size-exclusion chromatography performed in combination with analyses of static light scattering, ultraviolet absorbance, and refractive index using protocols described in Slotboom et al. (Slotboom et al., 2008). Each purified protein, at a final concentration of 0.5-1.5mg/ml, was clarified by centrifugation at 200,000xg for 30 minutes before crystallization.

2.5 Set up of the 96-well micro-volume dialysis crystallization plate

A protein concentration of 0.3-0.6mg/ml and a volume of 15–25μl were employed per crystallization condition. Thus ~0.4-1mg of a membrane protein target was needed to set up a complete 96-condition screen. Aliquots of 15–25μl of the purified membrane protein at different lipid-to-protein ratios were prepared in 96-well disposable microtiter plates, adding the protein solution last. These samples were incubated for 1h at room temperature to ensure a homogeneous population of protein/detergent/lipid micelles. Thereafter, each sample was transferred to individual sample wells of the microfluidic dialysis plate. This commercially available (XZ-HT-96) 96-well micro-volume dialysis crystallization plate was designed by GN Biosystems (Santa Clara, CA) and can accommodate sample and buffer volumes of 5–

28μl and up to 500μl, respectively. The MWCO of the dialysis membrane ranged from 12,000 to 14,000Da. Following the addition of the protein and buffer, the plates were film sealed and incubated at the desired dialysis temperature. Buffer was exchanged twice a day for a period of up to two weeks. After removing the sealing film the samples were recovered through slits at the top of each dialysis chamber and transferred to a 96-well disposable microtiter plate. As an alternative to the 96-well micro-volume dialysis crystallization plate a fraction of the conditions were also set up in 20μl dialysis buttons against 50ml dialysis buffer for detergent removal (Stokes et al., 2010).

2.6 Automated EM analysis of crystallization trials

Our automated pipeline to screen membrane protein 2D crystallization has been described elsewhere (Kim et al., 2010), and more details can be found at http://temimps.nysbc.org/technology.htm., or at the Structural Biology Knowledgebase (http://www.sbkb.org). In brief, batches of 100 carbon coated EM grids were prepared as described in Vink et al. (Vink et al., 2007). For automated negative staining, the EM grids were manually transferred onto a magnetic support platform (SPRI plate 384 Post Magnet Plate, Agencourt, Beverly MA) that was placed on a liquid-handling robot (Biomek FX, Beckman Coulter, Fullerton, CA). The staining of 2μl of each crystallization condition using a solution of 0.25% uranyl acetate in water was carried out by the liquid-handling robot using a 96-pipette head as previously described (Kim et al., 2010). The specimen grids were then manually transferred to a custom-made storage tray for automated grid insertion into the electron microscope and image acquisition (Hu et al., 2010). The specimen grids were inserted with a two-part robot consisting of a selective compliance articulated robot arm (SCARA) for loading samples into a microscope holder containing a modified tip, and a Cartesian robot for placing the holder into the electron microscope. A standard 120 keV JEOL-1230 transmission electron microscope (JEOL USA Inc.) modified with a rewired toggle switch controlling the airlock to allow robot control was used. A computer program for controlling the robots was integrated with the Leginon program (Potter et al., 1999;Suloway et al., 2005), which provides a module for automated imaging of individual samples. Images for each grid corresponding to an individual crystallization condition were taken in an unattended manner from regions of interest selected by the ANIMATED-TEM algorithms developed by Coudray et al. (Coudray et al., 2011). The resulting images are uploaded into the Sesame laboratory information management system (Zolnai et al., 2003), where they are associated with other data relevant to the crystallization screen (Hu et al., 2010).

3. Results and Discussion

All together we used ~250 screens from ~200 journal articles to construct a database of successful 2D crystallization conditions, which is freely accessible at http://www.sesame.wisc.edu/ using the Jafar module. Figure 1A depicts the resolution of the 2D crystals in the database as a function of their type. With 47% of the entries planar 2D crystals or sheets produced the highest resolution. These crystals, characterized by a planar bilayer with a coherent 2D array of proteins, are relatively large in both dimensions and are favored for a 3D analysis of their structure. Related vesicular crystals, arising from flattened lipid vesicles containing two overlapping 2D lattices, constitute 17% of the entries, and tend

to produce lower resolution than sheets since their rectangular shape and smaller size affects tilted data collection. Finally with 36% of the entries, tubular crystals, characterized by an array of proteins with helical symmetry in a cylindrical lipid vesicle that provides many different views of the molecules and thus do not need to be tilted, can also produce high-resolution 3D structures. With 70% of entries the vast majority of the 2D crystals in the database were produced by detergent dialysis, followed by detergent adsorption by bio-beads with 15% of entries, and with the lipid monolayer technique, complexation by cyclodextrin, dilution, or a combination of these methods accounting for the remaining 15% of entries.

3.1 Membrane proteins used in the analysis

The database included 2D crystallization experiments from a total of 12 β-barrel and 138 α-helical membrane proteins. Approximately 50% of these proteins were from bacteria, 45% from eukaryotes, and 5% from archaea. Two thirds of all the α-helical membrane proteins had 4–12 transmembrane domains, while the largest protein complexes contained 20–60 transmembrane domains and up to 5,000 amino acid residues. We grouped these proteins into seven different functional families (Fig. 1B). The largest families are the transporters and the channels, followed by photosynthetic proteins, ATPases and respiratory proteins. GPCRs and membrane enzymes are also present, but account for less than 10% of the entries in each case.

3.2 Detergent selection for 2D crystallization

Detergents are amphipathic molecules, consisting of a polar head group and a hydrophobic chain, capable of solubilizing membrane proteins by creating a mimic of a lipid bilayer environment. In general the choice of detergent is a critical factor for the initial solubilization and subsequent purification, and even functional characterization of a membrane protein. In addition, the detergent plays a prominent role in the formation and stabilization of the detergent/protein/lipid ternary complexes that constitute the starting point in a 2D crystallization experiment. The detergent is also critical during the reconstitution of the membrane protein into lipid bilayers, as its interactions with lipids and protein play an important role during this process (Rigaud et al., 2000). However, after reconstitution of the lipid bilayer, the role of detergent becomes less prominent as protein-protein and protein-lipid interactions dominate in the formation of well-ordered lattices. Indeed, detergent is only a minor component of the final 2D crystal. Despite a great deal of effort to understand the effect of detergent on membrane proteins, there is no single detergent that can be generally and reliably applied. Indeed, in numerous cases, the detergent used for the initial extraction and purification will not be effective in preserving function or in promoting the formation of well diffracting 2D crystals. Thus the choice of detergent must be made empirically.

Figure 2A shows the top twelve detergents that to date have been successfully used in 2D crystallization. These data show a clear preference for the alkyl maltopyranoside detergents, accounting for ~30% of the entries in the database, followed by the alkyl glucopyranoside detergents with ~18% of the entries. Of the alkyl maltopyranoside detergents, n-Dodecyl-β-D-maltopyranoside (DDM) is as successful as n-Decyl-β-D-maltopyranoside (DM).

Regarding the alkyl glucopyranosides, n-Octyl-β-D-glucopyranoside (OG) is clearly the most successful, whereas n-Hexyl-β-D-glucopyranoside (HG), n-Heptyl-β-D-thioglucopyranoside (HTG), and n-Octyl-β-D-thioglucopyranoside (OTG) have been seldom used. The alkyl polyoxyethylene detergents were also successful with ~18% of the entries in the database. Of these detergents, α-[4-(1,1,3,3-Tetramethylbutyl)phenyl]-ω-hydroxy-poly(oxy-1,2-ethanediyl) (Triton X-100) appears to be the most successful. We note that although the detergents OG, DDM and DM are also commonly used in 3D crystallization, the detergent Triton X-100 is seldom employed, as it is polydisperse and has a rather large micelle that tends to interfere with lattice formation. Likely, its prominence in 2D crystallization reflects the fact that Triton X-100 is very efficient at solubilization, forming mixed micelles of detergent and lipid at relatively low concentrations without the formation of complex intermediate aggregates (López et al., 1998). Because the detergent is ultimately removed, the properties of the micelle are not as important to the outcome of 2D crystallization. With regard to detergent concentration, a relatively wide range has been used for 2D crystallization with a median value of 3.4x the critical micelle concentration (CMC). In rare cases, the detergent concentration can be as high as 130xCMC, though more typical values are 2xCMC for high CMC-detergents, such as OG and DM, and up to 5.7xCMC for low-CMC detergents such as DDM and Triton X-100.

Our analysis did not yield clear correlations between physicochemical properties of the proteins and the detergents that could help predict outcomes for future 2D crystallization trials. This is not surprising, as previous attempts by X-ray crystallographers to establish meaningful correlations between membrane proteins and detergents in 3D crystallization have also not been successful (Newstead et al., 2008). However, we noted several interesting trends. The detergent OG has been successful in 2D crystallization primarily with membrane proteins displaying an average negative electrical charge at pH 7.0, while the opposite is true for DM. The rational for this observation is unclear as both detergents are nonionic. We also note that 75% of proteins in our database that were successfully crystallized from OG or tetraethylene glycol monooctyl ether (C8E4) have less than 8 transmembrane helices. In addition, 70% of the proteins crystallized from either of these two detergents have a molecular weight below 40 kDa, while only 27% of the proteins crystallized from other detergents have such low molecular weight. One possible explanation for these observations is that the relatively short alkyl chain of both OG and C8E4 affects the ability of these detergents to solubilize membrane proteins that are very hydrophobic or that contain a large number of transmembrane helices. In support of this idea, a recent study (White et al., 2008) tested the extraction of 122 yeast membrane proteins in 6 detergents - n-Dodecyl-N,N-Dimethylamine-N-Oxide (LDAO), DDM, OG, and C8E4, 1-Dodecanoyl-2-Hydroxy-sn-Glycero-3-Phosphocholine (FC12) and Triton X-100 - and found that the short-chain detergents were, in general, the least effective. They also reported that as the number of transmembrane domains and the molecular weight of the proteins increased, the more difficult it was to solubilize them in OG or C8E4. Finally, the authors also underlined that OG and C8E4 were less effective as the percentage of charged and polar amino acids (EDKRHNQST) in the transmembrane region increased. Interestingly, we have neither found in our database any protein successfully crystallized from these two detergents when the percentage of charged and polar amino acids is above 20%. An alternative explanation is

that although OG and C8E4 may solubilize the larger or more highly charges proteins, they are unstable in the micelles and thus aggregate during purification.

3.3 Lipid selection for 2D crystallization

The choice of lipid is another key factor in 2D crystallization. Lipids can have two distinct roles. Arranged in a bilayer, phospholipids provide a physical environment for reconstitution. Even as bilayers, phospholipids can adopt a variety of morphologies determined by the structure of the lipid, the nature of the lipid headgroup and its degree of hydration, the degree of unsaturation of the fatty acid chains, lateral pressure, temperature, ionic strength, and pH. As a consequence, the physical chemistry that governs the reconstitution of a membrane protein in a bilayer is complex, and thus the choice of lipid must ultimately be made empirically. However, we do know that it is energetically unfavorable for membrane proteins to expose their hydrophobic regions to water, or to embed hydrophilic regions in the hydrocarbon core of the lipid bilayer; thus, the hydrophobic regions of phospholipid and proteins need to be matched (Mouritsen and Bloom, 1993). Lipids can also fulfill an additional role as specific ligands. Indeed, individual lipids are often found bound to specific sites in membrane proteins (Wiener, 2006;Hunte and Richers, 2008), being essential for their structural integrity and functional activity (Dowhan, 1997).

Figure 2B shows the top twelve lipids that to date have been successfully used in 2D crystallization. These data show a clear preference for phosphatidylcholine lipids, accounting for over 65 % of the entries in the database. Polar and total lipid extracts from E. coli, composed mainly of phosphatidylethanolamine and phosphatidylglycerol lipids in a 8:2 ratio, were the next most successful with 20% of the entries. Of the phosphatidylcholine lipids, dimyristoylphosphatidylcholine (DMPC: 14:0) had most entries in the database, followed by dioleoylphosphatidylcholine (DOPC: 18:1) and palmytyl-oleoylphosphatidylcholine (POPC: 16:0/18:1). Natural lipid extracts rich in DOPC and POPC, such as egg-yolkPC and soybeanPC have also been used successfully in 10% and 7% of the cases, respectively.

As was the case with the detergents discussed above, we did not observe clear correlations between physicochemical properties of proteins and lipids in 2D crystallization. We note, however, that the vast majority of β-barrel membrane proteins - found only in prokaryotic membranes and in mitochondria - have been crystallized in either DMPC or E. coli lipid extracts. In contrast, DOPC a lipid often used to crystallize α-helical membrane proteins has not been used successfully with β-barrel membrane proteins. We also note that thylakoid lipids have been used exclusively in the crystallization of PSII complexes. Indeed, lipids used for 2D crystallization generally reflect the composition of native membranes, though given the relatively limited number of proteins represented in this database and the general lack of high-throughput methodologies employed for 2D crystallization, we believe it would be interesting to explore a broader range of lipids (e.g., cardiolipin and sphingomyelin) in future screens.

3.4 The lipid to protein ratio in 2D crystallization

The lipid to protein ratio (LPR) is another critical variable in 2D crystallization. If the lipid content is too high, then the protein will not be sufficiently concentrated in the plane of the lipid bilayer to induce 2D crystallization. Alternatively, if the lipid concentration is too low, the membrane protein target will aggregate and denature upon detergent removal. In principle, one should be able to precisely control the LPR in the initial protein/detergent/lipid ternary mixture. In reality, however, the purified membrane protein carries unpredictable amounts of bound lipids derived from the host membrane (Zhao et al., 2010;De Zorzi et al., 2013). Therefore, most laboratories will initially screen a broad range of LPRs followed by a more exhaustive sampling once crystallization hits are identified.

On a weight per weight basis the LPRs that have been successfully used in 2D crystallization vary from 0.1 to 1.5 without a clear peak or specific distribution. However, the LPR expressed on a mol per mol basis is more informative as it shows a unimodal distribution with a peak around a LPR of 25 (Fig. 3A). Despite the fact that the LPR generally increases as the number of transmembrane domains increases (Fig. 3B), the peak at a LPR of ~25 remains valid for membrane proteins with 6–14 transmembrane domains. When the LPR is estimated from the dimensions of the unit cell of a 2D crystal - by using a cross section area of $1nm^2$ for a α-helix and $0.6nm^2$ for a phospholipid - a correlation between LPR and the number of transmembrane domains is even more striking with distinct peaks at LPRs of ~25 and ~40 for membrane proteins with 8 and 12 transmembrane domains, respectively (Fig. 3C). Given that two thirds of all the α-helical membrane proteins in the database had 4–12 transmembrane domains these observations are broadly relevant to future crystallization screens.

What could be the role of these lipids? According to the insight on protein-lipid interactions derived from high-resolution electron crystallography structures, approximately half of these lipids will likely play a role as annular lipids to form a shell around the protein and engage in transient and relatively nonspecific interactions with the protein. The remaining half will constitute the bulk of the bilayer. Indeed, in the structure of bacteriorhodopsin at 3.5Å resolution (Grigorieff et al., 1996), 10 lipids were visible at the perimeter of each monomer (bacteriorhodopsin has 7 transmembrane helices), while additional lipids outside this shell could not be quantified. The structure of aquaporin-0 from eye lens at 1.9Å resolution revealed a belt of nine well-defined lipid molecules at the perimeter of each protein monomer (aquaporin-0 has 6 transmembrane helices) (Gonen et al., 2005;Hite et al., 2008). The aquaporin-0 structure also revealed lipids outside the shell of annular lipids, which lacked direct interactions with the protein and thus constituted the bulk of the bilayer.

3.5 pH in 2D crystallization

As with 3D crystallization the pH can have a significant impact on 2D crystallization. Figure 4A shows the success rate in 2D crystallization as a function of pH, with 60% of the entries in the database falling within the range of pH 7–8, and 13% of the entries clustering at around pH 6. Further analysis of the data revealed a positive correlation between the isoelectric point (pI) of the protein and the pH (Fig. 4B), in line with previous observations

made by Kantardjieff at al. (Kantardjieff and Rupp, 2004) in their analysis of 3D crystallization factors for soluble proteins reported in the Protein Data Bank.

3.6 Type and concentration of salts in 2D crystallization

Ions can often be essential for 3D crystallization as they can affect protein conformation, protein-protein interactions, and protein solubility. In the context of 2D crystallization, divalent cations are known to promote the stability of the phospholipid bilayer. Specifically, because they intercalate between the polar head group regions of phospholipids, divalent cations shield electrostatic repulsions between negatively charged phosphate regions. Of the various salts represented in the database NaCl, KCl, $MgCl_2$, and $CaCl_2$ have been the most successful (Fig. 5A). NaCl in combination with $MgCl_2$ accounts for over 60% of entries. In general, divalent salts are used at a lower concentration than monovalent salts. Polyvalent cations and ions can also serve as substrates and cofactors for transporters, channels and enzymes. In these cases, they can stabilize a particular protein intermediate and thus lock in a conformation that is amenable for 2D crystallization. In several examples, including PS II core (da Fonseca et al., 2002), BetP (Tsai et al., 2007), bovine lens connexin (Lampe et al., 1991), cyt b6f (Mosser et al., 1997), NanC (Signorell et al., 2007), GalP (Zheng et al., 2010), and aquaporin-2 (Schenk et al., 2005) the addition of specific divalent cations was crucial for 2D crystallization.

As part of our analysis we also explored a possible correlation between the ionic strength (IS) of a crystallization condition and the grand average of hydropathicity (GRAVY) for the protein. As shown in Figure 5B our analysis suggests a positive correlation between α-helical membrane proteins with a positive GRAVY and a high IS during 2D crystallization. Several specific examples illustrate this observation. For instance, 50 mM NaCl (IS = 0.05) yielded optimal crystals of CtrA3 (GRAVY = 0.137) (Chintalapati et al., 2008). In the case of aquaporin-8 (GRAVY = 0.67) a 100 mM NaCl (IS = 0.1) was necessary (Agemark et al., 2012), whereas GalP (GRAVY = 0.6) crystallized in a combination of 150 mM NaCl, 25 mM $CaCl_2$ and 25 mM $MgCl_2$ (IS = 0.23) (Zheng et al., 2010). Finally, the Enzyme IIC mannitol (GRAVY = 0.87) yielded the best crystals when the IS was 0.3 or above, while at lower IS the crystals deteriorated (Stuart et al., 2004).

3.7 Temperature in 2D crystallization

The predominant lipid bilayer form in biological membranes is the lamellar liquid crystalline phase (L_α which is characterized by considerable disorder in the acyl chains. Below a transition temperature characteristic of the particular lipid, the acyl chains are packed more tightly together giving rise to the lamellar gel phase (L_β) and a higher overall lipid density within the bilayer. Our analysis shows that the majority of membrane protein 2D crystallization has been carried out at constant temperatures above this transition temperature.

Room temperature (20–27°C) has been successful in 46% of the entries in the database (51% if we consider the 20–30°C range), followed by low temperature (4°C) with 16% and high temperature (37°C) with 8% of the entries. Cycling the temperature above and below the transition temperature has also been shown to be effective in 17% of the entries. In rare

cases, other temperatures (8°C, 12°C and 50°C) or cycling between 4°C and room temperature have also been used. Aside from its effect on the phase transition of the lipid bilayer, temperature can also affect the stability of the target protein, and the rate of detergent removal through dialysis. At low temperatures the protein of interest might be more stable during 2D crystallization, which can take several days and up to two weeks, but the phase transition of lipids containing DMPC might be affected and the dialysis rates of detergent slowed. In contrast, at high temperatures not all proteins might be stable, but it is possible to shorten the experiment duration by increasing the detergent removal rate and favoring crystallization by increasing Brownian motion.

3.8 Design of sparse and incomplete factorial 2D crystallization matrices

Based on our analysis of successful 2D crystallization conditions reported in the literature, we have designed a targeted sparse matrix crystallization screen. We applied the k-means algorithm to form 10 groups derived from 94 successful 2D crystallization conditions from 57 unique membrane proteins. The resulting matrix comprises 10 conditions, which is intended to be screened at 3 to 6 different LPRs, depending on the amount of protein available (Table 1). While the three most successful lipids (E.coli polar extract, DMPC and DOPC) are well represented in the screen, it also includes a few other species. The pH range of 6–8 covers ~75% of the entries in the database, the divalent salt concentration is kept low, as in ~80% of the entries, and the NaCl concentrations cover the most successful 50–300 mM range. Thus with 30 conditions, this targeted sparse matrix screen allows one to survey a significant portion of the published 2D crystallization space.

Incomplete factorial or grid screens offer an alternative to maximize the exploration of crystallization space. Designed to optimize the screening of a large amount of factors in as few experiments as possible, these screens have become increasingly popular in 3D crystallization (DeLucas et al., 2003;Luft et al., 2011). Using the most important factors affecting 2D crystallization, we designed an incomplete factorial 2D crystallization screen of 90 conditions (Table 2). In combination with 6 control conditions, this screen is compatible with the conventional 96-well high-throughput format.

The incomplete factorial screen covers a large variety of lipid polar head groups, acyl chain lengths and levels of unsaturation. In addition, mixtures of lipids are well represented in the screen, either as the principal constituents of the bilayer or as more specific protein co-factors. For instance, we included cholesterol in the screen as it has been used as a co-factor to improve the quality and reduce the aggregation of rhodopsin 2D crystals (Mielke et al., 2002), and is known to stabilize other membrane proteins. Brain lipid extract, rich in sphingolipids and gangliosides, is also included as a co-factor in several of the conditions. The distribution of LPRs efficiently cover a wide range of observed values, and pHs between 4.5–9 cover ~100% of the entries in the database and the majority of the physiological pH range available for protein and lipids. The concentrations of divalent salts (Ca^{2+} and Mg^{2+}) is kept in the 5–50 mM range, and the monovalent salt type and concentration range explores known 2D crystallization space. In addition, additives known to stabilize proteins such as glycerol and (β-mercaptoethanol (β-ME) are also sampled as they have been found to influence the size and order of BetP (Tsai et al., 2007) and

glutathione transferase (Schmidt-Krey et al., 1998) 2D crystals. Finally, in this screen we have also tried to sample various kinetics of detergent removal. In some cases, 2D crystallization can occur concomitantly with reconstitution of the membrane protein into a lipid bilayer. However, in other cases, crystallization occurs after reconstitution has finished. This entire process depends on the relative kinetics of detergent removal and crystal formation, as well as on the physical nature of the intermolecular interactions that stabilize the crystal lattice (Rigaud et al., 2000;Rigaud and Lévy, 2003). The CMC of a detergent is a key factor affecting the kinetics of detergent removal. Detergents having a CMC > 0.1% (w/w) can be eliminated by dialysis in less than a week, whereas low CMC (< 0.05%) detergents require significantly longer dialysis times. The low CMC detergents are also good candidates for adsorption by hydrophobic resins such as Biobeads (Rigaud et al., 1997), or complexation by cyclodextrins (Signorell et al., 2007). Indeed, α-, β- or γ-cyclodextrins can be used to remove low CMC detergents from lipid/detergent/protein ternary mixtures to facilitate the reconstitution and crystallization of membrane proteins, and we have therefore included cyclodextrin in the dialysis buffer of some of the conditions. In addition, our matrix also incorporates microdialysis buttons, as the larger area of their dialysis membrane relative to the crystallization plate as well as the higher buffer to sample volume ratio can also influence the kinetics of detergent removal. Finally, we explored the effect of detergent mixtures in 2D crystallization by virtue of using different detergents for membrane protein and lipid solubilization.

3.9 Screening results using the sparse and incomplete factorial 2D crystallization matrices

Crystallization was carried out by detergent dialysis in parallel on a 96-well format. Typically the screening of 2D crystallization trials involves four key steps: crystallization, specimen preparation for electron microscopy, image acquisition, and evaluation (Dreaden et al., 2013). We have incorporated all these steps into an automated pipeline that greatly improves throughput and reproducibility of the 2D crystallization process (Kim et al., 2010). For the implementation of the new sparse and incomplete factorial 2D crystallization matrices we have incorporated a new 96-well microfluidic dialysis plate into our crystallization pipeline. Our original 96-well dialysis block was built with standard 96-well SBS microplate dimensions and permitted the dialysis of 96 unique samples against 96 different buffers (Vink et al., 2007). This block could accommodate sample and buffer volumes of up to 53μl and 1ml respectively, and thus - at a typical protein concentration of 0.5 mg/ml - up to 2.5mg of protein were required for a full 96-condition 2D crystallization screen. In order to reduce the sample volume we have collaborated with GN Biosystems (Santa Clara, CA) to develop a microfluidic dialysis system for low-volume, high-throughput crystallization trials. This microfluidic dialysis plate can accommodate 5–28μl of sample per well and up to 500μl per buffer chamber. In our case, we have used 15–25μl of sample per well, the total amount of protein needed for a 96-condition screen would be reduced to approximately 0.4-1mg. Following dialysis for periods of up to two weeks, negatively stained specimens were prepared in parallel using a 96-position magnetic platform to hold EM grids and a liquid handling robot (Kim et al., 2010). Finally, robotic grid insertion into the electron microscope and computerized image acquisition (Hu et al., 2010) from regions of interest selected automatically (Coudray et al., 2011) ensured the rapid and reliable evaluation of the crystallization screen. The resulting images were

uploaded into the Sesame laboratory information management system (Zolnai et al., 2003). Currently, an experienced microscopist performs data analysis and evaluation, but efforts to automate these steps using algorithms for crystal detection and automated collection of diffraction data are underway.

To date, 19 2D crystallization screens have been performed on 16 different target membrane proteins (Table 3). This corresponds to over 1,300 individual crystallization experiments evaluated by over 50,000 EM images. Six membrane protein targets have yielded diffracting crystals (Table 3, Fig. 6). In all these successful cases, initial hits were observed in either the sparse matrix or incomplete factorial crystallization screens, which provided the basis for designing more focused screens to improve crystal quality and abundance. Out of the 12 membrane protein targets tested with the sparse matrix screen, 5 have produced crystals. Crystals for 4 out of 6 membrane protein targets have been obtained with the incomplete factorial screen. Some of the targets have yielded crystals with both screens, whereas other targets crystals could only be obtained with one of the screens. This relatively high success rate suggests that the new matrices presented here have good potential to accelerate the process of membrane protein 2D crystallization.

We note that the majority of 2D crystals produced by our screens had a tubular morphology. The helical symmetry underlying this tubular morphology offers an advantage for structure determination, because a full 3D dataset can be obtained without the need to tilt the crystals and because new iterative helical real-space refinement (IHRSR) procedures have proven effective in producing high resolution structures (Behrmann et al., 2012;Wu et al., 2014). Despite screening a wide-range of conditions, we were unable to obtain either vesicular or sheet crystals for all but one of our protein targets. This preference for tubular 2D crystals likely reflects constraints of the crystal lattice due either to the topology or to the intermolecular protein contacts of the crystallized targets. Specific inter-molecular associations within the detergent depleted protein-lipid aggregates may also govern the resulting crystal symmetry and morphology. In some cases, a given protein will form both tubular and planar crystals (Jap et al., 1992), indicating that there are alternative sets of crystal contacts that are differentially selected by the conditions during reconstitution and crystal growth. Presumably, the curvature of tubular crystals is the result of the differences in the distance of the protein-protein contacts on either side of the membrane that arise when membrane proteins are incorporated into the lipid bilayer with a unique orientation. In contrast, membrane proteins inserted in an "upside-down" orientation can have a two-fold symmetry axis oriented parallel to the membrane plane and often produce extended, planar crystals (e.g., light harvesting complex II (Kühlbrandt and Wang, 1991), cytochrome oxidase (Valpuesta et al., 1990), glutathione transferase (Holm et al., 2006)). By analyzing only the primary or predicted secondary structures of the screened proteins, it is not easy to foresee their propensity to form tubular crystals. The six proteins that, so far, have yielded tubular crystals have different topologies (4–17 transmembrane helices), hydrophobicities (37–69% intramembranous), and isoelectric points (4.6–10.3), as predicted through www.cbs.dtu.dk/services/TMHMM/ and au.expasy.org/tools/protparam.html. Thus, additional proteins need to be screened, and more ambitious bioinformatics studies conducted, in order to draw more generalized conclusions.

4. Conclusions

This communication presents an attempt to rationalize membrane protein 2D crystallization. Using information derived from our analysis we have designed two new 2D crystallization matrices that complement each other and combined allow the efficient sampling of a broad range of the multifactorial 2D crystallization space. In combination with available procedures to automate the steps of crystallization, specimen preparation for electron microscopy, image acquisition, and evaluation, these matrices can improve the odds for producing well-ordered 2D crystals of membrane proteins. Once initial hits are identified with the sparse and/or incomplete factorial crystallization matrices it may take multiple rounds of optimization to improve the quality and abundance of 2D crystals suitable for data collection by cryo-EM and structure determination. Optimization is certainly case-specific, however some general rules include: (1) fine-tuning of the crystallization factors around the initial hits; (2) varying the protein concentration; (3) addition of known protein ligands, substrates or inhibitors; (4) modifying the chromatographic steps for protein purification or removing purification tags; and (5) altering the kinetics of detergent removal by exploring alternative reconstitution techniques such as dilution (Dolder et al., 1996), adsorption by Biobeads (Rigaud et al., 1997) or complexation by cyclodextrins (Signorell et al., 2007).

From a technical perspective there have been recent important advances for high-throughput screening of 2D crystallization trials and for automated imaging of membrane crystals with the electron microscope (Cheng et al., 2007;Vink et al., 2007;Coudray et al., 2008;Hu et al., 2010;Iacovache et al., 2010;Karathanou et al., 2010;Kim et al., 2010;Coudray et al., 2011;Glover et al., 2011). In addition, there have also been very recent key developments in detector technologies capable of recording EM images with unprecedented signal-to-noise ratio (Liao et al., 2013). Finally, there have also been key developments in software to facilitate the process of structure determination (Hirai et al., 1999;Philippsen et al., 2003;Gipson et al., 2007;Philippsen et al., 2007;Diaz et al., 2010), including new IHRSR procedures for helical 2D crystals (Egelman, 2010;Behrmann et al., 2012) and a semi-automated structure determination pipeline with the software package 2dx for flat 2D crystals (Scherer et al., 2014). In combination with all these advances, the 2D crystallization matrices presented here will be valuable to affirm electron crystallography as a viable tool for routine structure determination of membrane proteins along side NMR spectroscopy and X-ray crystallography.

Acknowledgements

We are grateful to the laboratories of Dr. Tom Walz, Dr. Wayne Hendrickson, Dr. Tamir Gonen, and Dr. Robert Stroud, and the Center for Eukaryotic Structural Genomics for supplying some of the proteins used for 2D crystallization. Funding for this work was provided by grants U54GM094598 and R01GM095747 from the National Institutes of Health and grant MCB-1244236 from the National Science Foundation.

Abbreviations

β-CD	methyl-β-cyclodextrin
DMPC	dimyristoylphosphatidylcholine

DMPS	dimyristoylphosphatidylserine
DOPA	dioleoylphosphatidic acid
DOPC	dioleoylphosphatidylcholine
DOPE	dioleoylphosphatidylethanolamine
DOPG	dioleoylphosphatidylglycerol
DOPS	dioleoylphosphoserine
EggPA	egg-yolk phosphatidic acid
EggPC	egg-yolk phosphatidylcholine
POPC	palmytyl-oleoylphosphatidylcholine
POPE	palmytyl-oleoylphosphatidylethanolamine
soyPC	soybean phosphatidylcholine
C8E4	tetraethylene glycol monooctyl ether
C12E8	octaethyleneglycol mono-n-dodecylether
C8POE	octyl- polyoxyethylene
CHAPS	3-[(3-Cholamidopropyl)dimethylammonio]-1-propanesulfonate
DDM	n-Dodecyl-b-D-maltopyranoside
DHPC	diheptanoylphosphocholine
DM	n-Decyl-b-D-maltopyranoside
FC12	1-Dodecanoyl-2-Hydroxy-sn-Glycero-3-Phosphocholine
HG	n-hexyl-beta-D-glucopyranoside
HTG	n-Heptyl beta-Dthioglucopyranoside
LDAO	n-Dodecyl-N,NDimethylamine-N-Oxide
OG	n-Octyl-beta-D-glucopyranoside
OTG	n-Octyl-beta-D-thioglucopyranoside
TDC	taurodeoxycholate
Triton X-100	α-[4-(1,1,3,3-Tetramethylbutyl)phenyl]-ω-hydroxy-poly(oxy-1,2-ethanediyl)

References

Abeyrathne PD, Chami M, Pantelic RS, Goldie KN, Stahlberg H. Preparation of 2D crystals of membrane proteins for high-resolution electron crystallography data collection. Methods in Enzymology. 2012; 481:25–43. [PubMed: 20887851]

Agemark M, Kowal J, Kukulski W, Nordén K, Gustavsson N, Johanson U, Engel A, Kjellbom P. Reconstitution of water channel function and 2D-crystallization of human aquaporin 8. Biochimica et Biophysica Acta - Biomembranes. 2012; 1818:839–850.

Behrmann E, Tao G, Stokes DL, Egelman EH, Raunser S, Penczek PA. Real-space processing of helical filaments in SPARX. Journal of Structural Biology. 2012; 177:302–313. [PubMed: 22248449]

Carter CW Jr, Carter CW. Protein crystallization using incomplete factorial experiments. J Biol Chem. 1979; 254:12219–12223. [PubMed: 500706]

Carter C Jr. Efficient factorial designs and the analysis of macromolecular crystal growth conditions. Methods. 1990; 1:12–24.

Cheng A, Leung A, Fellmann D, Quispe J, Suloway C, Pulokas J, Abeyrathne P, Lam J, Carragher B, Potter C. Towards automated screening of two-dimensional crystals. Journal of Structural Biology. 2007; 160:324–331. [PubMed: 17977016]

Chintalapati S, Alkurdi R, Terwisschavanscheltinga A, Kuhlbrandt W. Membrane Structure of CtrA3, a Copper-transporting P-type-ATPase from Aquifex aeolicus. J Mol Biol. 2008; 378:581–595. [PubMed: 18374940]

Coudray N, Beck F, Buessler J, Korinek A, Karathanou A, Remigy H, Kihl H, Engel A, Plizko J, Urban J. Automatic Acquisition and Image Analysis of 2D Crystals. Microscopy Today. 2008; 16:48–49.

Coudray N, Hermann G, Caujolle-Bert D, Karathanou A, Erne-Brand F, Buessler JL, Daum P, Plitzko JM, Chami M, Mueller U, Kihl H, Urban JP, Engel A, Remigy HW. Automated screening of 2D crystallization trials using transmission electron microscopy: a high-throughput tool-chain for sample preparation and microscopic analysis. J Struct Biol. 2011; 173:365–374. [PubMed: 20868753]

da Fonseca P, Morris EP, Hankamer B, Barber J. Electron crystallographic study of photosystem II of the cyanobacterium Synechococcus elongatus. Biochemistry. 2002; 41:5163–5167. [PubMed: 11955064]

De Zorzi R, Nicholson WV, Guigner JM, Erne-Brand F, Venien-Bryan C. Growth of large and highly ordered 2D crystals of a K(+) channel, structural role of lipidic environment. Biophys J. 2013; 105:398–408. [PubMed: 23870261]

DeLucas LJ, Bray TL, Nagy L, McCombs D, Chernov N, Hamrick D, Cosenza L, Belgovskiy A, Stoops B, Chait A. Efficient protein crystallization. J Struct Biol. 2003; 142:188–206. [PubMed: 12718931]

Diaz R, Rice WJ, Stokes DL. Chapter Five - Fourier-Bessel Reconstruction of Helical Assemblies. Methods in Enzymology. 2010; 482:131–165. [PubMed: 20888960]

Dolder M, Engel A, Zulauf M. The micelle to vesicle transition of lipids and detergents in the presence of a membrane protein: towards a rationale for 2D crystallization. FEBS Lett. 1996; 382:203–208. [PubMed: 8612753]

Dowhan W. Molecular basis for membrane phospholipid diversity: why are there so many lipids? Annu Rev Biochem. 1997; 66:199–232. [PubMed: 9242906]

Dreaden, TM.; Metcalfe, M.; Kim, LY.; Johnson, MC.; Barry, BA.; Schmidt-Krey, I. Screening for Two-Dimensional Crystals by Transmission Electron Microscopy of Negatively Stained Samples. In: Ingeborg, YC., editor. Electron Crystallography of Soluble and Membrane Proteins : Methods and Protocols. Vol. 955. Schmidt-Krey: Humana Press; 2013. p. 73-101.

Egelman EH. Reconstruction of helical filaments and tubes. Methods Enzymol. 2010; 482:167–183. [PubMed: 20888961]

Gipson B, Zeng X, Zhang Z, Stahlberg H. 2dx—User-friendly image processing for 2D crystals. Journal of Structural Biology. 2007; 157:64–72. [PubMed: 17055742]

Glover CA, Postis VL, Charalambous K, Tzokov SB, Booth WI, Deacon SE, Wallace BA, Baldwin SA, Bullough PA. AcrB contamination in 2-D crystallization of membrane proteins: lessons from a sodium channel and a putative monovalent cation/proton antiporter. J Struct Biol. 2011; 176:419–424. [PubMed: 21964467]

Gonen T, Cheng Y, Sliz P, Hiroaki Y, Fujiyoshi Y, Harrison SC, Walz T. Lipid-protein interactions in double-layered two-dimensional AQP0 crystals. Nature. 2005; 438:633–638. [PubMed: 16319884]

Gorrec F, Palmer CM, Lebon G, Warne T. Pi sampling: a methodical and flexible approach to initial macromolecular crystallization screening. Acta Crystallogr D Biol Crystallogr. 2011; 67:463–470. [PubMed: 21543849]

Grigorieff N, Ceska TA, Downing KH, Baldwin JM, Henderson R. Electron-crystallographic refinement of the structure of bacteriorhodopsin. J Mol Biol. 1996; 259:393–421. [PubMed: 8676377]

Henderson R, Unwin PN. Three-dimensional model of purple membrane obtained by electron microscopy. Nature. 1975; 257:28–32. [PubMed: 1161000]

Hirai T, Murata K, Mitsuoka K, Kimura Y, Fujiyoshi Y. Trehalose embedding technique for high-resolution electron crystallography: application to structural study on bacteriorhodopsin. J Electron Microsc (Tokyo). 1999; 48:653–658. [PubMed: 15603052]

Hite RK, Gonen T, Harrison SC, Walz T. Interactions of lipids with aquaporin-0 and other membrane proteins. Pflugers Arch. 2008; 456:651–661. [PubMed: 17932686]

Holm P, Bhakat P, Jegerschold C, Gyobu N, Mitsuoka K, Fujiyoshi Y, Morgenstern R, Hebert H. Structural Basis for Detoxification and Oxidative Stress Protection in Membranes. J Mol Biol. 2006; 360:934–945. [PubMed: 16806268]

Hu M, Vink M, Kim C, Derr K, Koss J, D'Amico K, Cheng A, Pulokas J, Ubarretxena-Belandia I, Stokes D. Automated electron microscopy for evaluating two-dimensional crystallization of membrane proteins. J Struct Biol. 2010; 171:102–110. [PubMed: 20197095]

Hunte C, Richers S. Lipids and membrane protein structures. Curr Opin Struct Biol. 2008; 18:406–411. [PubMed: 18495472]

Iacovache I, Biasini M, Kowal J, Kukulski W, Chami M, van der Goot FG, Engel A, Rémigy HW. The 2DX robot: a membrane protein 2D crystallization Swiss Army knife. Journal of Structural Biology. 2010; 169:370–378. [PubMed: 19963066]

Jancarik J, Scott WG, Milligan DL, Koshland DE Jr, Kim SH. Crystallization and preliminary X-ray diffraction study of the ligand-binding domain of the bacterial chemotaxis-mediating aspartate receptor of Salmonella typhimurium. J Mol Biol. 1991; 221:31–34. [PubMed: 1656050]

Jap BK, Zulauf M, Scheybani T, Hefti A, Baumeister W, Aebi U, Engel A. 2D crystallization: from art to science. Ultramicroscopy. 1992; 46:45–84. [PubMed: 1481277]

Kantardjieff KA, Rupp B. Protein isoelectric point as a predictor for increased crystallization screening efficiency. Bioinformatics. 2004; 20:2162–2168. [PubMed: 14871873]

Karathanou A, Coudray N, Hermann G, Buessler JL, Urban JP. Automatic TEM image analysis of membranes for 2D crystal detection. Adv Exp Med Biol. 2010; 680:327–333. [PubMed: 20865516]

Kim C, Vink M, Hu M, Love J, Stokes DL, Ubarretxena-Belandia I. An automated pipeline to screen membrane protein 2D crystallization. J Struct Funct Genomics. 2010; 11:155–166. [PubMed: 20349145]

Kühlbrandt W. Two-dimensional crystallization of membrane proteins. Q Rev Biophys. 1992; 25:1–49. [PubMed: 1589568]

Kühlbrandt W, Wang DN. Three-dimensional structure of plant light-harvesting complex determined by electron crystallography. Nature. 1991; 350:130–134. [PubMed: 2005962]

Lampe PD, Kistler J, Hefti A, Bond J, Muller S, Johnson RG, Engel A. In vitro assembly of gap junctions. J Struct Biol. 1991; 107:281–290. [PubMed: 1666956]

Liao M, Cao E, Julius D, Cheng Y. Structure of the TRPV1 ion channel determined by electron cryo-microscopy. Nature. 2013; 504:107–112. [PubMed: 24305160]

López O, de la Maza A, Coderch L, López-Iglesias C, Wehrli E, Parra JL. Direct formation of mixed micelles in the solubilization of phospholipid liposomes by Triton X-100. FEBS Letters. 1998; 426:314–418. [PubMed: 9600258]

Luft JR, Wolfley JR, Snell EH. What's in a drop? Correlating observations and outcomes to guide macromolecular crystallization experiments. Cryst Growth Des. 2011; 11:651–663.

Mielke T, Villa C, Edwards PC, Schertler GFX, Heyn MP. X-ray diffraction of heavy-atom labelled two-dimensional crystals of rhodopsin identifies the position of cysteine 140 in helix 3 and cysteine 316 in helix 8. J Mol Biol. 2002; 316:693–709. [PubMed: 11866527]

Mosser G. Two-dimensional crystallogenesis of transmembrane proteins. Micron. 2001; 32:517–540. [PubMed: 11163725]

Mosser G, Breyton C, Olofsson A, Popot JL, Rigaud JL. Projection map of cytochrome b6 f complex at 8 A resolution. Journal of Biological Chemistry. 1997; 272:20263–20268. [PubMed: 9242706]

Mouritsen OG, Bloom M. Models of lipid-protein interactions in membranes. Annu Rev Biophys Biomol Struct. 1993; 22:145–171. [PubMed: 8347987]

Newstead S, Ferrandon S, Iwata S. Rationalizing alpha-helical membrane protein crystallization. Protein Science. 2008; 17:466–472. [PubMed: 18218713]

Philippsen A, Schenk AD, Signorell GA, Mariani V, Berneche S, Engel A. Collaborative EM image processing with the IPLT image processing library and toolbox. J Struct Biol. 2007; 157:28–37. [PubMed: 16919967]

Philippsen A, Schenk AD, Stahlberg H, Engel A. Iplt--image processing library and toolkit for the electron microscopy community. J Struct Biol. 2003; 144:4–12. [PubMed: 14643205]

Potter CS, Chu H, Frey B, Green C, Kisseberth N, Madden TJ, Miller KL, Nahrstedt K, Pulokas J, Reilein A, Tcheng D, Weber D, Carragher B. Leginon: a system for fully automated acquisition of 1000 electron micrographs a day. Ultramicroscopy. 1999; 77:153–161. [PubMed: 10406132]

Remigy HW, Caujolle-Bert D, Suda K, Schenk A, Chami M, Engel A. Membrane protein reconstitution and crystallization by controlled dilution. FEBS Lett. 2003; 555:160–169. [PubMed: 14630337]

Rigaud J, Chami M, Lambert O, Levy D, Ranck J. Use of detergents in two-dimensional crystallization of membrane proteins. Biochim Biophys Acta. 2000; 1508:112–128. [PubMed: 11090821]

Rigaud J-L, Lévy D. Reconstitution of membrane proteins into liposomes. Meth Enzymol. 2003; 372:65–86. [PubMed: 14610807]

Rigaud JL, Mosser G, Lacapere JJ, Olofsson A, Levy D, Ranck JL. Bio-Beads: an efficient strategy for two-dimensional crystallization of membrane proteins. J Struct Biol. 1997; 118:226–235. [PubMed: 9169232]

Rupp B, Wang J. Predictive models for protein crystallization. Methods. 2004; 34:390–407. [PubMed: 15325656]

Schenk AD, Werten PJ, Scheuring S, de Groot BL, Muller SA, Stahlberg H, Philippsen A, Engel A. The 4.5 A structure of human AQP2. J Mol Biol. 2005; 350:278–289. [PubMed: 15922355]

Scherer S, Kowal J, Chami M, Dandey V, Arheit M, Ringler P, Stahlberg H. 2dx_automator: implementation of a semiautomatic high-throughput high-resolution cryo-electron crystallography pipeline. J Struct Biol. 2014; 186:302–307. [PubMed: 24680783]

Schmidt-Krey I, Lundqvist G, Morgenstern R, Hebert H. Parameters for the two-dimensional crystallization of the membrane protein microsomal glutathione transferase. J Struct Biol. 1998; 123:87–96. [PubMed: 9843664]

Signorell GA, Chami M, Condemine G, Schenk AD, Philippsen A, Engel A, Remigy HW. Projection maps of three members of the KdgM outer membrane protein family. J Struct Biol. 2007; 160:395–403. [PubMed: 17919922]

Signorell GA, Kaufmann TC, Kukulski W, Engel A, Remigy HW. Controlled 2D crystallization of membrane proteins using methyl-beta-cyclodextrin. J Struct Biol. 2007; 157:321–328. [PubMed: 16979348]

Slotboom DJ, Duurkens RH, Olieman K, Erkens GB. Static light scattering to characterize membrane proteins in detergent solution. Methods. 2008; 46:73–82. [PubMed: 18625320]

Stokes DL, Rice WJ, Hu M, Kim C, Ubarretxena-Belandia I. Two-dimensional crystallization of integral membrane proteins for electron crystallography. Methods Mol Biol. 2010; 654:187–205. [PubMed: 20665267]

Stuart MCA, Koning RI, Oostergetel GT, Brisson A. Mechanism of formation of multilayered 2D crystals of the Enzyme IIC-mannitol transporter. Biochimica et Biophysica Acta - Biomembranes. 2004; 1663:108–116.

Suloway C, Pulokas J, Fellmann D, Cheng A, Guerra F, Quispe J, Stagg S, Potter CS, Carragher B. Automated molecular microscopy: the new Leginon system. J Struct Biol. 2005; 151:41–60. [PubMed: 15890530]

Tsai C-J, Ejsing CS, Shevchenko A, Ziegler C. The role of lipids and salts in two-dimensional crystallization of the glycine-betaine transporter BetP from Corynebacterium glutamicum. Journal of Structural Biology. 2007; 160:275–286. [PubMed: 17981051]

Ubarretxena-Belandia I, Stokes DL. Present and future of membrane protein structure determination by electron crystallography. Adv Protein Chem Struct Biol. 2010; 81:33–60. [PubMed: 21115172]

Ubarretxena-Belandia I, Stokes DL. Membrane protein structure determination by electron crystallography. Curr Opin Struct Biol. 2012; 22:520–528. [PubMed: 22572457]

Valpuesta JM, Henderson R, Frey TG. Electron cryo-microscopic analysis of crystalline cytochrome oxidase. J Mol Biol. 1990; 214:237–251. [PubMed: 2164584]

Vink M, Derr K, Love J, Stokes DL, Ubarretxena-Belandia I. A high-throughput strategy to screen 2D crystallization trials of membrane proteins. Journal of Structural Biology. 2007; 160:295–304. [PubMed: 17951070]

White MA, Clark KM, Grayhack EJ, Dumont ME. Characteristics Affecting Expression and Solubilization of Yeast Membrane Proteins. J Mol Biol. 2008; 365:621–636. [PubMed: 17078969]

Wiener, MC. A Census of Ordered Lipids and Detergents in X-ray Crystal Structures of Integral Membrane Proteins. Weinheim: Wiley-VCH Verlag GmbH & Co; 2006.

Wu B, Peisley A, Tetrault D, Li Z, Egelman EH, Magor KE, Walz T, Penczek PA, Hur S. Molecular Imprinting as a Signal-Activation Mechanism of the Viral RNA Sensor RIG-I. Mol Cell. 2014; 55:511–523. [PubMed: 25018021]

Zhao G, Johnson MC, Schnell JR, Kanaoka Y, Haase W, Irikura D, Lam BK, Schmidt-Krey I. Two-dimensional crystallization conditions of human leukotriene C4 synthase requiring adjustment of a particularly large combination of specific parameters. J Struct Biol. 2010; 169:450–454. [PubMed: 19903529]

Zheng H, Taraska J, Merz AJ, Gonen T. The prototypical H+/galactose symporter GalP assembles into functional trimers. J Mol Biol. 2010; 396:593–601. [PubMed: 20006622]

Zolnai Z, Lee PT, Li J, Chapman MR, Newman CS, Phillips GN Jr, Rayment I, Ulrich EL, Volkman BF, Markley JL. Project management system for structural and functional proteomics: Sesame. J Struct Funct Genomics. 2003; 4:11–23. [PubMed: 12943363]

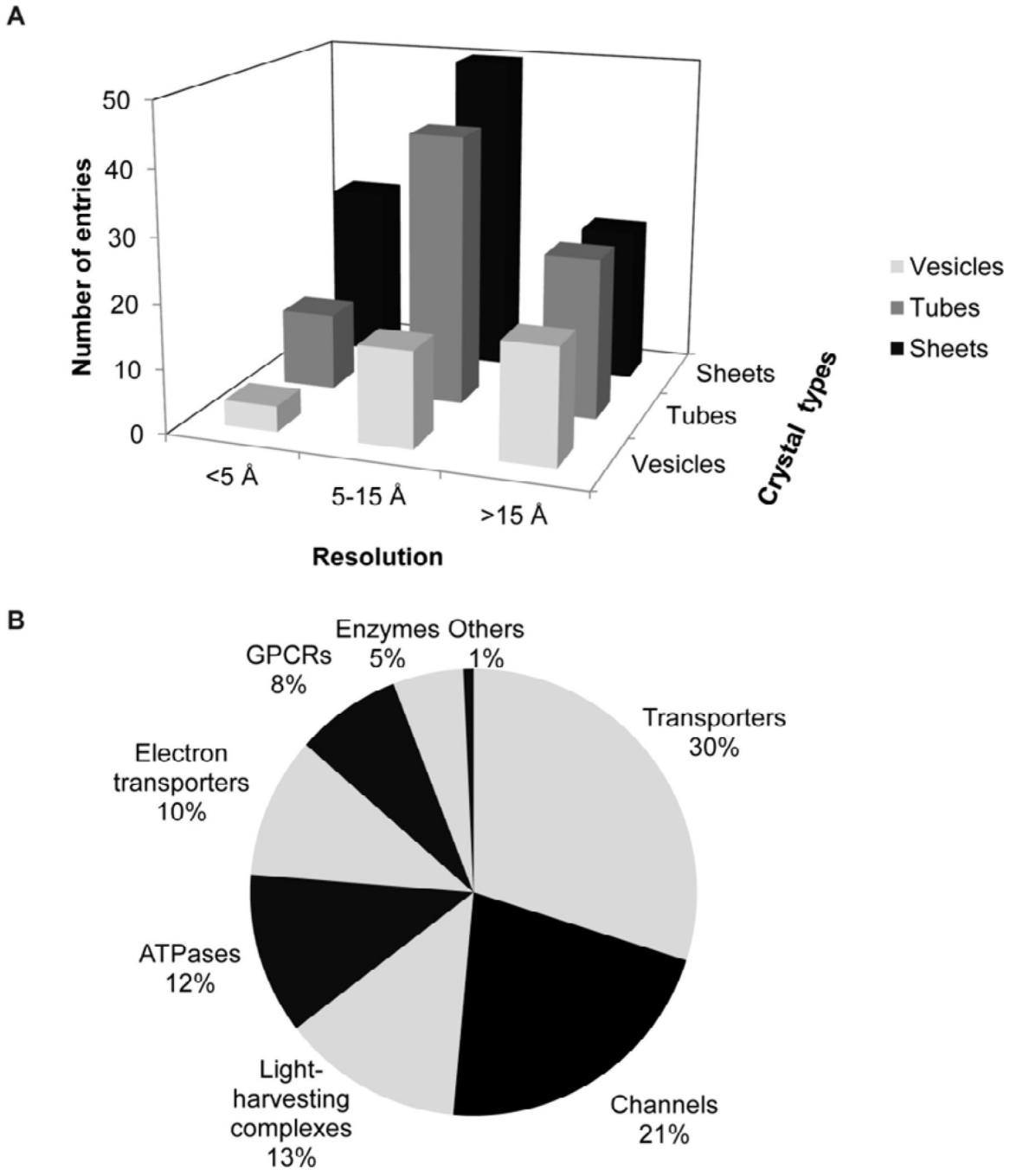

Figure 1. Types of 2D crystals and membrane protein families

A. The type, distribution and resolution of crystals in the 2D crystallization database. Depending on the publication resolution may refer to the final resolution of a 3D structure, 2D projection map, or diffraction pattern. **B**. The functional classification and distribution of the different membrane protein families in the 2D crystallization database.

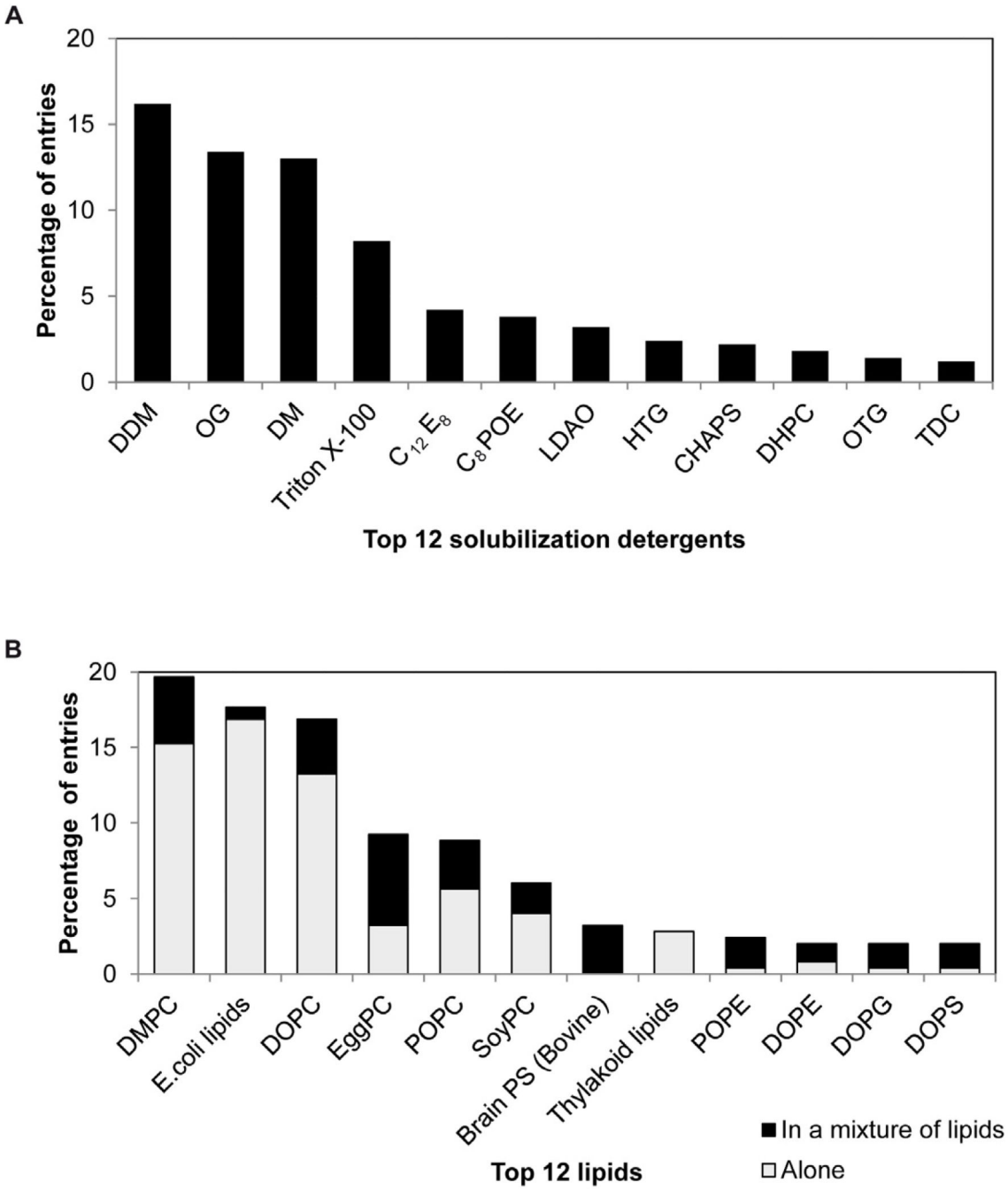

Figure 2. Detergent and lipid

A. The twelve most frequent detergents in the 2D crystallization database. In approximately 66% of the entries, both membrane protein and lipid were solubilized in the same detergent, whereas in the remaining entries a different detergent was used. **B**. The twelve most frequent lipids in the 2D crystallization database. E. coli* denotes E. coli polar lipid extract.

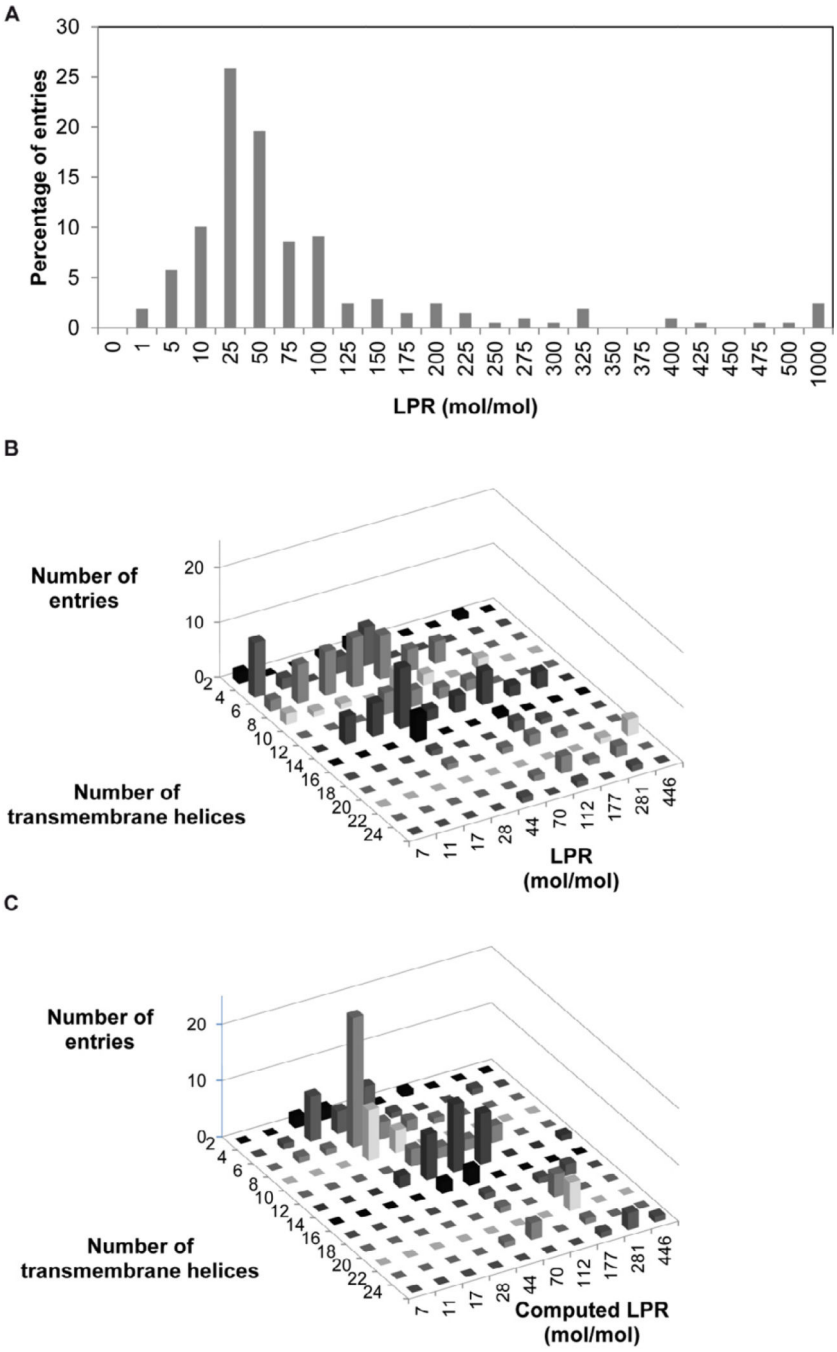

Figure 3. Lipid to protein ratio

A. The distribution of lipid to protein ratios (LPRs) in mol per mol in the 2D crystallization database. **B**. The distribution of LPRs as a function of the number of number of transmembrane helices. **C**. The distribution of LPRs calculated from the dimensions of the unit cell of a 2D crystal (using a cross section area of $1nm^2$ for a α-helix and $0.6nm^2$ for a phospholipid) as a function of the number transmembrane helices.

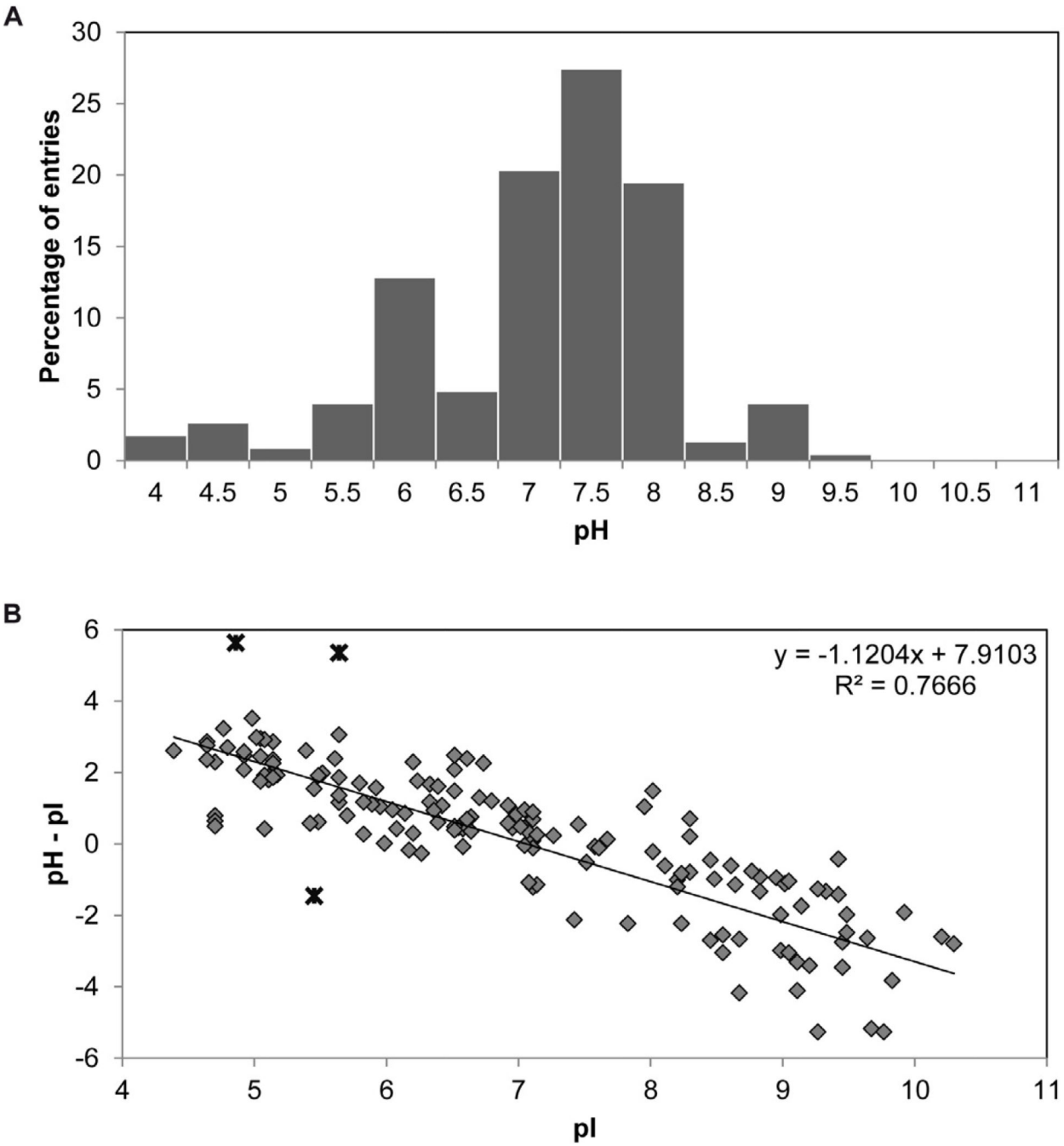

Figure 4. pH

A. Distribution of pHs in the 2D crystallization database. **B**. Positive correlation between the pI of the membrane proteins in the database and the pH used in 2D crystallization.

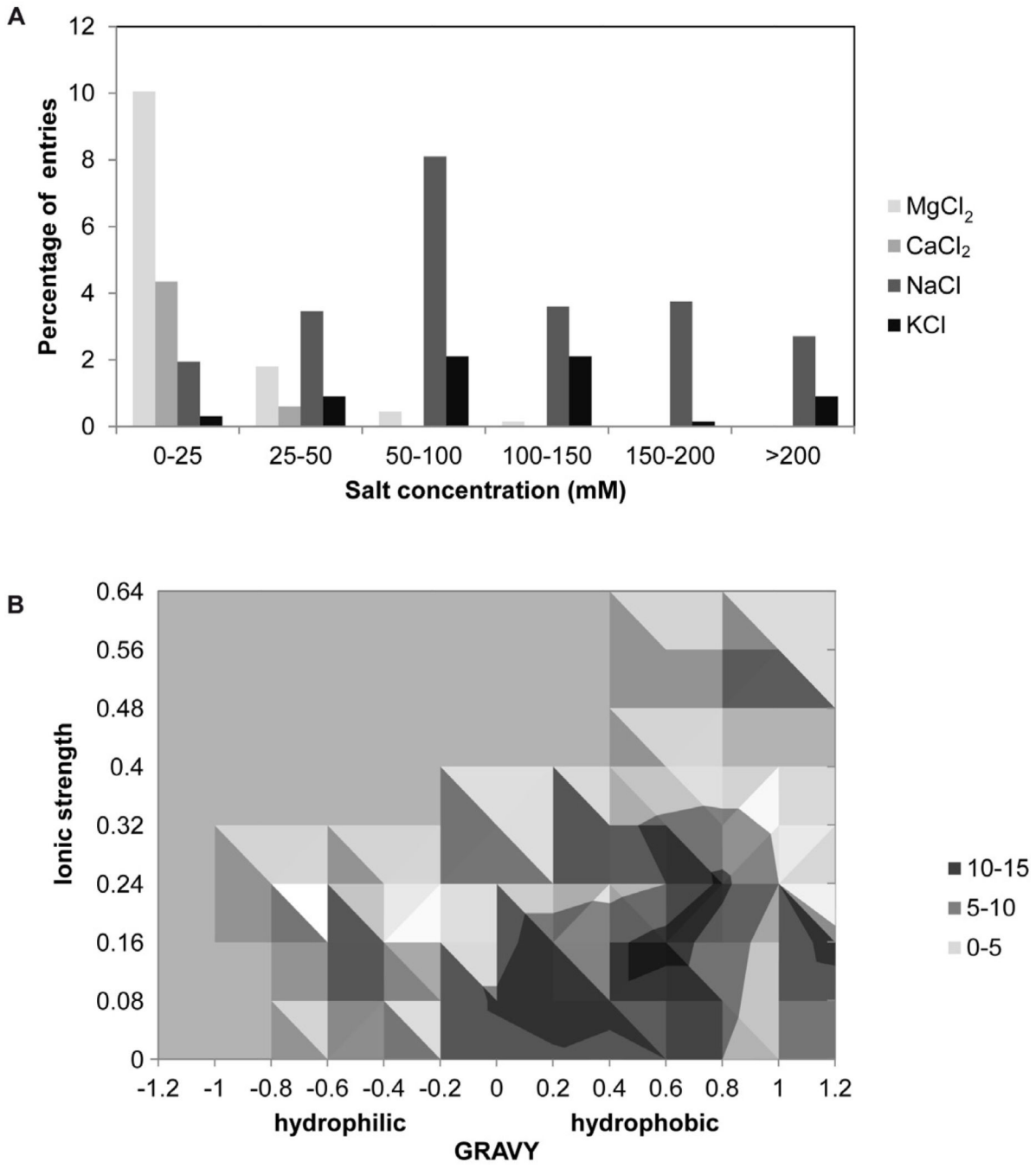

Figure 5. Salts

A. The distribution of the concentrations of the prevalent salts (in the crystallization buffers) in the 2D crystallization database. **B**. The ionic strength (IS) in 2D crystallization as a function of the grand average of hydropathicity (GRAVY). The data suggests a positive correlation in 2D crystallization between helical membrane proteins with a positive GRAVY value and a high IS.

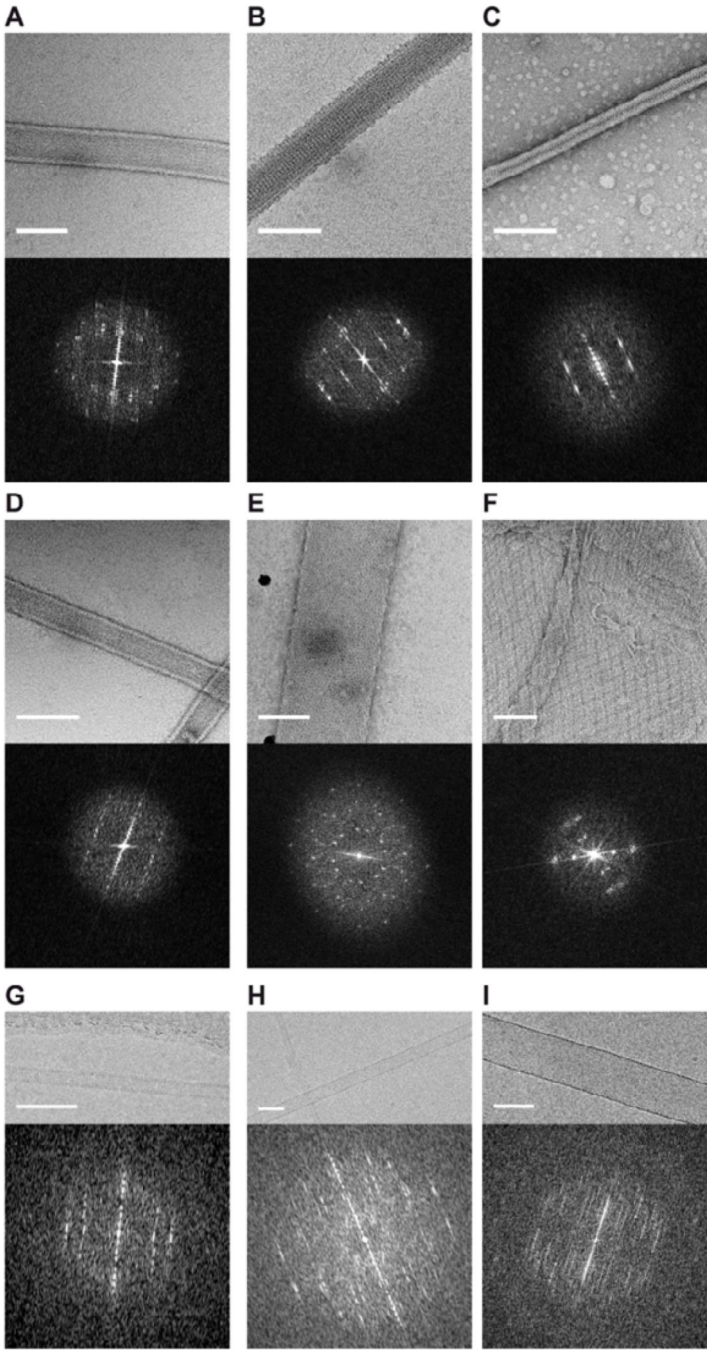

Figure 6. Gallery of 2D crystals obtained using the sparse and incomplete factorial matrices

Images show negatively stained helical crystals of three different transporters (**A, B, C**) one enzyme (**D**) and one channel (**E**), and a crystalline vesicle of a channel (**F**). Cryo images of some of the targets are also shown (**G, H, I**). The scale bars are 100 nm.

Table 1

Sparse matrix 2D crystallization screen.

Condition #	Lipids	Temperature	pH	$MgCl_2$ [mM]	NaCl [mM]
1	E.coli polar	cycle	6	50	100
2	E.coli polar	RT	7.5	2	150
3	DOPC	cycle	7.5	0	100
4	DOPC	4°C	7	10	100
5	DMPC	RT	7	0	300
6	DMPC:DOPC (1:4)	cycle	7	40	150
7	DMPC:DMPS (8.5:1.5)	RT	8	2	50
8	DOPC:DOPA (9:1)	RT	7.5	0	200
9	EggPC	RT	6	2	50
10	DOPE	RT	7.5	0	100

RT = room temperature; cycle = temperature cycling between 12 h at 27°C and 12 h at 37°C. The lipid ratios are given in weight.

Table 2

Incomplete factorial matrix 2D crystallization screen.

Buffer	Lipid	Co-factor	LPR	Monovalent Salt	Divalent Salt	Detergent	Detergent removal	Additive	Temp
pH6.5 MES	EggPC/DOPS	none	1.5	250mM Na_2SO_4	5mM $CaCl_2$	C12E8	µdia+5mM β-CD	2% glycerol	4°C
pH7.5 HEPES	DOPG	10% cholesterol	0.1	250mM KCl	5mM $MgCl_2$	DDM	µdia+5mM β-CD	2% glycerol	4°C
pH5.5 Citrate	DMPC	10% brain extract	0.1	150mM Na_2HPO_4	50mM $CaCl_2$	DDM	µdia+5mM β-CD	none	4°C
pH6.5 MES	E.coli polar	10% cholesterol	0.3	150mM NaCl	5mM $MgCl_2$	TritonX100	µdia+5mM β-CD	2% glycerol	4°C
pH8.5 Tris	DOPG	10% cholesterol	0.5	250mM NaCl	5mM $CaCl_2$	C12E8	µdia+1 mM β-CD	none	4°C
pH5.0 Citrate	SoyPC	none	1.3	50mM NaCl	none	DM	µdia+1 mM β-CD	none	4°C
pH5.5 Citrate	E.coli polar	10% cholesterol	1.1	150mM KCl	50mM $MgCl_2$	OG	µdia+1 mM β-CD	5mM B-MEA	4°C
pH7.0 HEPES	EggPC/EggPA	10% brain extract	0.3	150mM Na_2HPO_4	5mM $MgCl_2$	OG	µdia+1 mM β-CD	none	4°C
pH4.5 Citrate	DMPC	10% cholesterol	0.3	150mM Na_2SO_4	5mM $CaCl_2$	TritonX100	µdia+1 mM β-CD	none	4°C
pH6.5 MES	SoyPC	10% brain extract	0.5	150mM Na_2SO_4	50mM $MgCl_2$	DDM	µdia	5mM B-MEA	4°C
pH5.5 Citrate	EggPC/DOPS	10% cholesterol	0.7	50mM KCl	5mM $CaCl_2$	DM	µdia	2% glycerol	4°C
pH6.0 MES	DMPC	none	0.1	50mM Na_2HPO_4	5mM $CaCl_2$	OG	µdia	2% glycerol	4°C
pH9.0 Tris	POPC	none	1.3	150mM KCl	50mM $CaCl_2$	TritonX100	µdia	2% glycerol	4°C
pH7.0 HEPES	EggPC/EggPA	10% cholesterol	0.9	250mM mM NaCl	50mM $MgCl_2$	TritonX100	µdia	2% glycerol	4°C
pH7.0							µdia+5mM β-	5mM B-	

Buffer	Lipid	Co-factor	LPR	Monovalent Salt	Divalent Salt	Detergent	Detergent removal	Additive	Temp
HEPES	POPC	10% cholesterol	1.3	50mM Na_2HPO_4	5mM $CaCl_2$	DDM	CD	MEA	20°C
pH5.0 Citrate	EggPC/DOPS	10% cholesterol	1.5	50mM Na_2SO_4	5mM $CaCl_2$	DM	µdia+5mM β-CD	2% glycerol	20°C
pH4.5 Citrate	SoyPC	none	0.9	50mM Na_2HPO_4	5mM $MgCl_2$	DM	µdia+5mM β-CD	none	20°C
pH7.0 HEPES	EggPC/DOPS	none	0.1	250mM Na_2HPO_4	50mM $MgCl_2$	TritonX100	µdia+5mM β-CD	5mM B-MEA	20°C
pH8.0 Tris	DOPC	10% brain extract	0.5	50mM KCl	50mM $MgCl_2$	TritonX100	µdia+5mM β-CD	2% glycerol	20°C
pH6.0 MES	DOPG	10% brain extract	0.9	250mM Na_2SO_4	50mM $MgCl_2$	DDM	µdia+1 mM β-CD	none	20°C
pH6.5 MES	EggPC/EggPA	10% cholesterol	1.1	250mM Na_2HPO_4	none	DM	µdia+1 mM β-CD	2% glycerol	20°C
pH8.0 Tris	EggPC/EggPA	none	1.5	50mM Na_2SO_4	50mM $CaCl_2$	OG	µdia+1 mM β-CD	5mM B-MEA	20°C
pH5.5 Citrate	DOPC	10% brain extract	0.1	50mM NaCl	5mM $MgCl_2$	OG	µdia+1 mM β-CD	2% glycerol	20°C
pH8.5 Tris	DMPC	10% cholesterol	1.3	50mM Na_2SO_4	5mM $MgCl_2$	C12E8	µdia	5mM B-MEA	20°C
pH9.0 Tris	SoyPC	10% brain extract	0.5	150mM NaCl	none	C12E8	µdia	5mM B-MEA	20°C
pH6.5 MES	POPC	none	0.9	50mM KCl	50mM $CaCl_2$	OG	µdia	none	20°C
pH6.0 MES	DOPC	10% cholesterol	1.5	150mM KCl	none	TritonX100	µdia	none	20°C
pH9.0 Tris	EggPC/EggPA	10% brain extract	0.7	50mM NaCl	5mM $CaCl_2$	C12E8	µdia+5mM β-CD	5mM B-MEA	27°C
pH8.0 Tris	EggPC/DOPS	10% cholesterol	0.9	150mM Na_2SO_4	none	C12E8	µdia+5mM β-CD	2% glycerol	27°C
pH5.0 Citrate	POPC	10% brain extract	0.1	150mM KCl	5mM $MgCl_2$	C12E8	µdia+5mM β-CD	none	27°C

Buffer	Lipid	Co-factor	LPR	Monovalent Salt	Divalent Salt	Detergent	Detergent removal	Additive	Temp
pH8.5 Tris	E.coli polar	10% brain extract	1.5	150mM Na_2SO_4	50mM $CaCl_2$	DDM	µdia+5mM β-CD	5mM B-MEA	27°C
pH8.0 Tris	SoyPC	10% cholesterol	1.3	250mM KCl	50mM $MgCl_2$	OG	µdia+5mM β-CD	none	27°C
pH8.0 Tris	E.coli polar	none	0.1	250mM NaCl	5mM $CaCl_2$	DDM	µdia+1 mM β-CD	5mM B-MEA	27°C
pH4.5 Citrate	POPC	10% cholesterol	0.7	250mM NaCl	50mM $MgCl_2$	DM	µdia+1 mM β-CD	2% glycerol	27°C
pH9.0 Tris	EggPC/DOPS	none	0.5	50mM Na_2SO_4	5mM $MgCl_2$	DM	µdia+1 mM β-CD	none	27°C
pH5.0 Citrate	DOPC	none	0.3	250mM NaCl	50mM $CaCl_2$	DDM	µdia	2% glycerol	27°C
pH5.0 Citrate	EggPC/DOPS	10% brain extract	0.7	150mM NaCl	5mM $CaCl_2$	OG	µdia	5mM B-MEA	27°C
pH6.5 MES	DOPG	none	1.5	150mM Na_2HPO_4	50mM $MgCl_2$	OG	µdia	none	27°C
pH7.5 HEPES	DMPC	none	0.9	50mM NaCl	50mM $MgCl_2$	TritonX100	µdia	5mM B-MEA	27°C
pH7.5 HEPES	EggPC/EggPA	10% cholesterol	0.1	250mM Na_2SO_4	none	TritonX100	µdia	none	27°C
pH4.5 Citrate	DOPC	none	1.1	250mM NaCl	5mM $CaCl_2$	C12E8	µdia+5mM β-CD	5mM B-MEA	37°C
pH8.5 Tris	DOPC	none	0.7	150mM Na_2HPO_4	none	DDM	µdia+5mM β-CD	none	37°C
pH7.0 HEPES	DMPC	10% cholesterol	0.5	250mM Na_2SO_4	50mM $CaCl_2$	DM	µdia+5mM β-CD	5mM B-MEA	37°C
pH6.0 MES	SoyPC	10% cholesterol	1.1	150mM Na_2HPO_4	50mM $CaCl_2$	C12E8	µdia+1 mM β-CD	5mM B-MEA	37°C
pH8.0 Tris	DMPC	none	1.5	150mM NaCl	50mM $MgCl_2$	C12E8	µdia+1 mM β-CD	2% glycerol	37°C

Buffer	Lipid	Co-factor	LPR	Monovalent Salt	Divalent Salt	Detergent	Detergent removal	Additive	Temp
HEPES pH7.5	SoyPC	10% cholesterol	0.7	150mM KCl	5mM $MgCl_2$	DDM	CD µdia+1 mM β-	2% glycerol	37°C
HEPES	POPC	10% cholesterol	1.5	250mM Na_2HPO_4	5mM $CaCl_2$	OG	CD	2% glycerol	
pH4.5 Citrate	E.coli polar	10% brain extract	1.3	50mM KCl	none	TritonX100	µdia+1 mM β- CD	5mM B-MEA	37°C
pH5.0 Citrate	EggPC/EggPA	none	0.5	50mM Na_2HPO_4	50mM $CaCl_2$	TritonX100	µdia+1 mM β- CD	none	37°C
pH4.5 Citrate	DOPC	10% cholesterol	0.1	50mM Na_2SO_4	50mM $CaCl_2$	C12E8	µdia	none	37°C
pH9.0 Tris	DOPG	none	1.1	150mM Na_2SO_4	5mM $MgCl_2$	DDM	µdia	2% glycerol	37°C
pH6.0 MES	POPC	10% brain extract	0.5	150mM Na_2HPO_4	5mM $MgCl_2$	DM	µdia	2% glycerol	37°C
pH7.0 HEPES	DOPC	10% brain extract	1.1	150mM NaCl	5mM $CaCl_2$	DM	µdia	none	37°C
pH5.5 Citrate	DOPG	10% brain extract	0.9	50mM Na_2HPO_4	none	OG	µdia	5mM B-MEA	37°C
pH8.5 Tris	E.coli polar	10% brain extract	0.9	250mM KCl	5mM $CaCl_2$	TritonX100	µdia	2% glycerol	cycle
pH4.5 Citrate	EggPC/DOPS	none	0.9	150mM Na_2HPO_4	none	DDM	µdia+5mM β-CD	2% glycerol	cycle
pH9.0 Tris	SoyPC	10% brain extract	1.5	250mM Na_2SO_4	none	DM	µdia+5mM β-CD	5mM B-MEA	cycle
pH8.5 Tris pH7.0	EggPC/EggPA	10% brain extract	0.9	150mM KCl	50mM $MgCl_2$	DM	µdia+5mM β-CD	2% glycerol 5mM B-	cycle
HEPES	DOPG	none	0.3	50mM KCl	none	OG	µdia+5mM β-CD	MEA	cycle
pH6.0 MES	E.coli polar	none	0.7	250mM Na_2HPO_4	5mM $MgCl_2$	OG	µdia+5mM β-CD	none	cycle
pH9.0 Tris	DMPC	10% brain extract	1.1	250mM NaCl	50mM $CaCl_2$	TritonX100	µdia+5mM β-CD	none	cycle

Buffer	Lipid	Co-factor	LPR	Monovalent Salt	Divalent Salt	Detergent	Detergent removal	Additive	Temp
pH6.0 MES	EggPC/DOPS	10% brain extract	1.5	150mM Na_2SO_4	50mM $CaCl_2$	C12E8	CD	none	e
							µdia+1 mM β-	5mM B-	cycl
pH5.5 Citrate	POPC	none	0.5	250mM KCl	none	DDM	CD	MEA	e
							µdia+1 mM β-	5mM B-	cycl
pH6.5 MES	DOPC	10% cholesterol	1.3	250mM Na_2SO_4	50mM $CaCl_2$	OG	CD	MEA	e
pH7.5						TritonX10	µdia+1 mM β-		cycl
HEPES	SoyPC	10% brain extract	0.3	50mM Na_2SO_4	5mM $CaCl_2$	0	CD	2% glycerol	e
	EggPC/EggPA							5mM B-	cycl
pH4.5 Citrate		none	1.1	250mM KCl	5mM $MgCl_2$	C12E8	µdia	MEA	e
									cycl
pH9.0 Tris	E.coli polar	10% cholesterol	0.3	50mM Na_2HPO_4	50mM $MgCl_2$	C12E8	µdia	none	e
								5mM B-	cycl
pH8.0 Tris	DOPG	10% cholesterol	0.7	50mM NaCl	50mM $CaCl_2$	DM	µdia	MEA	e
								5mM B-	4°C
pH8.0 Tris	POPC	10% brain extract	0.3	250mM Na_2HPO_4	none	C12E8	Button	MEA	
								5mM B-	4°C
pH6.0 MES	DOPC	none	0.3	250mM KCl	none	DM	Button	MEA	
pH7.0									4°C
HEPES	E.coli polar	10% brain extract	1.5	250mM KCl	50mM $CaCl_2$	DM	Button	none	
						TritonX10		5mM B-	4°C
pH8.5 Tris	POPC	none	1.1	250mM Na_2SO_4	5mM $MgCl_2$	0	Button	MEA	
pH7.5									20°C
HEPES	E.coli polar	none	0.5	150mM KCl	5mM $CaCl_2$	C12E8	Button	none	
								5mM B-	20°C
pH8.0 Tris	EggPC/DOPS	10% brain extract	1.1	150mM KCl	50mM $CaCl_2$	DDM	Button	MEA	
pH5.0 Citrate	DOPG	10% brain extract	1.1	50mM Na_2SO_4	none	DDM	Button	2% glycerol	20°C
pH7.5								5mM B-	20°C
HEPES	DOPC	none	0.7	150mM Na_2SO_4	50mM $MgCl_2$	DM	Button	MEA	
pH5.0 Citrate	DMPC	10% cholesterol	0.5	250mM KCl	none	OG	Button	2% glycerol	20°C
pH6.5 MES	DMPC	10% brain extract	0.7	50mM Na_2HPO_4	none	C12E8	Button	2% glycerol	27°C

Buffer	Lipid	Co-factor	LPR	Monovalent Salt	Divalent Salt	Detergent	Detergent removal	Additive	Temp
pH4.5 Citrate	DOPG	10% brain extract	1.3	250mM Na_2HPO_4	50mM $MgCl_2$	C12E8	Button	2% glycerol	27°C
pH5.5 Citrate	SoyPC	10% cholesterol	1.5	50mM KCl	5mM $MgCl_2$	DDM	Button	none	27°C
pH8.5 Tris	SoyPC	none	0.1	150mM NaCl	50mM $CaCl_2$	OG	Button	2% glycerol	27°C
						TritonX10		5mM B-	27°C
pH5.0 Citrate	E.coli polar	10% cholesterol	0.9	150mM Na_2HPO_4	5mM $MgCl_2$	0	Button	MEA	
	EggPC/EggP								37°C
pH5.5 Citrate	A	none	0.3	150mM Na_2SO_4	5mM $CaCl_2$	DM	Button	2% glycerol	
pH7.5								5mM B-	37°C
HEPES	EggPC/DOPS	10% brain extract	1.3	250mM NaCl	5mM $MgCl_2$	OG	Button	MEA	

LPR = Lipid-to-Protein Ratio (w/w); RT = room temperature; cycle = temperature cycling between 12 h at 27°C and 12 h at 37°C; detergent = detergent used for lipid solubilization; μdia = microdialysis plate; Button = dialysis buttons; β-CD = cyclodextrin; B-MEA: β-mercaptoethanol; The lipid ratios are given in weight. Ratio of EggPC/EggPA and EggPC/D.

Table 3

Summary of 2D crystallization trials.

Function	Organism	MW (kDa)	pI	TMD	TM (%)	Sparse	I.F.	Best outcome
ATPase	E.coli	154.7	7.2	21	31	Yes	No	Vesicles packed with protein
Channel	Rabbit	565.2	5.2	8	4	No	**Yes**	**Striated vesicles**
Channel	E.coli	49.7	9.7	12	54	No	Yes	Non-diffracting tubes
Channel	E.coli	37.1	4.6	17	55	**Yes**	**Yes**	**Diffracting helical tubes and crystalline sheets**
Enzyme	M.arvoryzae	33.6	8.9	7	52	**Yes**	No	**Rare striated sheets and non-diffracting tubes**
Enzyme	B.subtilis	24.0	8.9	7	69	**Yes**	No	**Diffracting helical tubes**
Other	Guinea pig	66.5	5.5	2	7	Yes	No	Sheet-like structure
Other	S.aureus	49.8	5.3	6	29	Yes	No	Vesicles, aggregates
Other	Mus musculus	24.8	8.1	4	38	Yes	No	Vesicles, aggregates
Other	Homo sapiens	22.0	8.8	4	42	Yes	No	Vesicles, aggregates
Transporter	I.loihiensis	28.1	9.5	4	37	No	**Yes**	**Diffracting helical tubes**
Transporter	S.oneidensis	32.5	5.4	6	43	**Yes**	**Yes**	**Diffracting helical tubes**
Transporter	E.coli	32.5	6.0	6	43	**Yes**	No	**Diffracting helical tubes**
Transporter	S.oralis	46.0	9.4	11	55	No	Yes	Rare non-diffracting filaments
Transporter	S.typhimurium	44.8	10.3	12	61	**Yes**	Yes	**Diffracting helical tubes, and some sheets**
Transporter	L.monocytogenes	20.4	9.9	6	65	Yes	No	Non-diffracting tubes

MW = molecular weight; pI: isoelectric point; TMD: number of predicted transmembrane domains α-helices or β-strands); %TM: % of transmembrane sequence as predicted using the prediction software TMHMM (http://www.cbs.dtu.dk/services/TMHMM/); Sparse = Sparse matrix; I.F. = incomplete factorial matrix. I.F. Yes/No = indicates if a matrix has been run or not.